UNIVERSITY OF CALIFORNIA,
IRVINE

CO_2 Capture and Concentration using Alkoxides and Photoacids

THESIS

Submitted in partial satisfaction of the requirements
for the degree of

MASTER OF SCIENCE

in Chemistry

by

Amanda L. Kummeth

Dissertation Committee:
Professor Jenny Yang, Chair
Professor Andy Borovik
Professor Shane Ardo

2022

Table of Contents

Acknowledgments

I would like to express my sincere appreciation for my committee, especially my chair, Professor Jenny Yang, for their support during my time at UCI.

Thanks to my lab mates and classmates for putting up with me and my puns.

Financial support was provided by Sloan Foundation and the University of California, Irvine.

ABSTRACT OF THESIS

CO_2 capture and concentration using alkoxides and photoacids

by

Amanda L. Kummeth

Master of Science in Chemistry

University of California, Irvine 2022

Professor Jenny Yang, Chair

With the increase of CO_2 and other greenhouse gases emissions into the atmosphere, research into methods to mitigate these emissions is gaining more attention. The use of various capture agents to absorb CO_2 from either waste gas streams or directly from air can lead to completely carbon-neutral or carbon-negative technologies. This work studies two new methods for CO_2 capture: a direct capture method using alkoxides, and an indirect capture method using photoacids for creating localized pH swings. CO_2 capture using alkoxides was verified through the formation of alkyl carbonates. The CO_2 absorption capacity was then measured for each alkoxide synthesized or purchased, showing a general trend for higher CO_2 absorption capacity correlating with higher pK_a values. The effect of the counter cation for alkoxides in CO_2 capture was also investigated, showing that changing the counter cation does in fact alter CO_2 absorption capacity for hydroxide (0.39-0.85 mole CO_2 absorbed per mole of hydroxide). The second capture system investigated used photoexcitation of photoacids to release captured CO_2 from solution. The initial setup to test CO_2 capture and release for this system shows effective CO_2 capture into solution and release of CO_2 after the photoacid is excited. However, this process's efficiency could be improved through use of a higher intensity photon source.

1. Introduction

The exponential increase of CO_2 in the atmosphere will not abate while the use of fossil fuels remains prevalent.[1] While research into utilizing CO_2 as a stock chemical through electro- and photocatalytic reduction is important, obtaining pure CO_2 for these reactions remains a challenge. To close the loop between CO_2 emission and CO_2 utilization, development of efficient CO_2 capture and concentration technologies for industrial waste gas, vehicle emissions, or directly from air is required.[2] Thus, it is imperative to create a system for CO_2 capture to work towards creating a carbon-neutral, or even carbon-negative, society.

Currently, the most developed method for CO_2 capture is thermal amine scrubbing where the waste gas stream from a post-combustion source (8-15% CO_2)[3,4] is sent through an absorber containing amine solution that reacts and captures CO_2 to form a carbamate salt (eqn 1).[5] The solution then flows to the desorber, where it is heated (110-130 ºC)[6], releasing gaseous CO_2 and regenerating the amine.

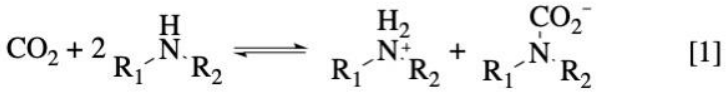

[1]

The amine most often used for thermal capture is monoethanolamine (MEA), a desirable capture agent due to its low cost and high rate of reaction.[5] While MEA degrades from the heat used in thermal amine scrubbing, its low cost makes it easy to replace. However, thermal regeneration is Carnot limited in energy efficiency; amine scrubbing is reliant on the introduction of external heat, resulting in high energetic costs that have prevented wide-spread application.[7,8] Other methods for CO_2 capture and concentration that do not rely on temperature swings include methods such as electrochemically mediated amine regeneration (EMAR),[6,9–13] electrochemical

pH swings,[14,15] electrochemical redox swings,[16–18] carbonate precipitation,[19] and gas capture into porous materials like metal organic frameworks.[20]

A process like electrochemical pH swings does not rely on heat and can be fully reversible, meaning it is theoretically 100% efficient. In addition, the energy required can be provided by solar power or other renewable energy sources, making these completely carbon-negative.[14–16] Proton-coupled electron transfer (PCET) pH-swing systems make use of a redox active molecule to adjust the concentration of protons in solution. For example, for a system developed by Jin *et al.*, CO_2 is first captured into an alkaline (pH ~ 13.5) aqueous solution through the formation of bicarbonate.[15] Then their redox active compound is reduced, releasing protons into the solution. The pH of the solution is further lowered, resulting in protonation of bicarbonate to carbonic acid. The equilibria at lower pH conditions favor H_2O and CO_2 over carbonic acid which allows the CO_2 to be released. The redox active species is then oxidized, which increases its basicity and alters the pH back to alkaline conditions.

2. CO_2 Capture using Alkoxides

2.1 Background

The generally accepted mechanism for CO_2 capture using amines requires that the amine acts as a nucleophile for dissolved CO_2.[21,22] As such, other nucleophiles could provide alternative routes for CO_2 capture, especially for direct air capture. While amines effectively capture CO_2 from sources with higher concentration of feedstock CO_2 (flue gas), there is less success of capture at lower concentrations of CO_2. Even so, some amines have been shown to capture CO_2 directly from air, at a concentration of 0.04% CO_2; however, the majority of these amines are embedded in a molecular organic framework structure or other heterogenous surfaces.[23–25]

Another challenge in amine capture is the stoichiometry for carbamate formation (eqn 1). The 2:1 (amine:CO_2) capture stoichiometry for amines enforces a restricted efficiency upon the system, since maximum carbamate formation is 50%. As such, using alkoxides as a capture agent could offer superior CO_2 capture.

$$RO^- + CO_2 \rightleftharpoons RCO_3^- \qquad [2]$$

Alkoxides react with CO_2 to form an alkyl carbonate with 1:1 stoichiometry (eqn 2) since the alkoxide is already in its active form. In addition, the range of pK_as offered by alkoxides could provide different reactivities due to a correlation of nucleophilicity and pK_a.[26,27] The bonding energetics of CO_2 versus proton binding of amines, alkoxides, and phenoxides were calculated using density functional theory (DFT) by the Alexandrova group at UCLA.[28] In contrast to the previously suggested zwitterionic mechanistic pathway for CO_2 absorption with an amine, the DFT calculations suggest that a neutral amine does not create a covalent bond with CO_2 based on the N-C bond length of 2.82 Å in Figure 1. However, after deprotonation of the amine, the amino group can covalently bind the CO_2 with a binding energy of -53.1 kcal/mol and N-C bond length of 1.43 Å.[28] Because neutral amines always being more basic than water, the amines must go through an autoionization process before they can reach their active capture state of the deprotonated amine.

$$2\,R_1R_2NH \rightleftharpoons R_1R_2NH_2^+ + R_1R_2N^-$$
$$R_1R_2N^- + CO_2 \rightleftharpoons R_1R_2NCOO^-$$

These calculations illustrate that the pK_{a2} of the amine, the pK_a of deprotonation, holds more influence over the binding of CO_2 than that of pK_{a1}.

$$R_1R_2NH_2^+ \overset{pK_{a1}}{\rightleftharpoons} R_1R_2NH \overset{pK_{a2}}{\rightleftharpoons} R_1R_2N^- \qquad [3]$$

The calculated binding constants of the amine and CO_2 to pK_{a1} has little correlation. Previous data comparing CO_2 absorption capacity to pK_{a1} also indicates little trend between pK_{a1} and CO_2 binding.[29] However, when calculated binding constants for the amine and CO_2 are plotted against pK_{a2}, there is a remarkedly more linear trend, which supports that carbamate formation occurs only with the deprotonated amine.

Since the pK_{a2} range for amines is 20-30 in water, amines can be water sensitive and prone to protonation. This is likely the reason for the few successful direct air capture amine-based systems. However, alkoxides with a pK_a of their conjugate acid under 15.4 (the pK_a of water) should remain in their active form in water. Even so, DFT calculations show that the tradeoff for this water stability results in lower calculated CO_2 binding constants for alkoxides and phenoxides. Since nitrogen is a more nucleophilic atom than oxygen, it is reasonable that the binding constant of CO_2 would be higher.

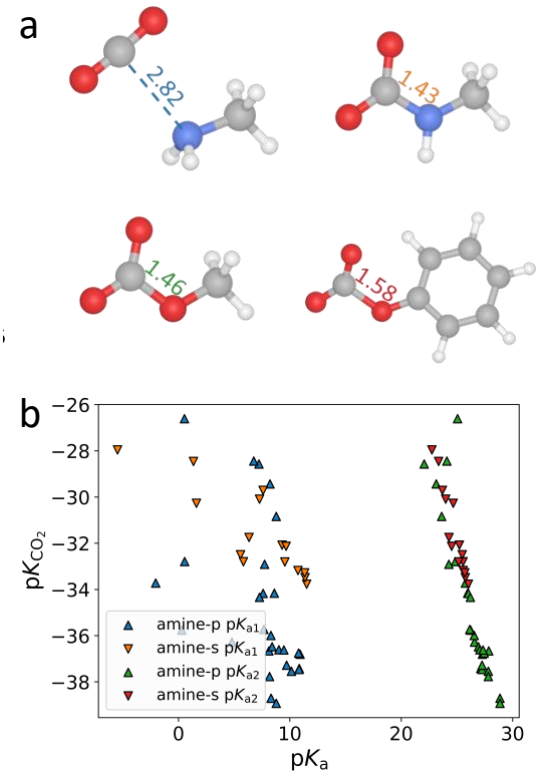

Figure 1. Energetics of CO_2 binding on capture agents from Zhang et al. a. Optimized geometries of CO_2 binding on $MeNH_2$, $MeNH^-$, MeO^-, and PhO^-, with the d(X-C) distances (X represent N for amine and O for alkoxide/phenoxide) labeled in Angstrom. b. Scatter plot of DFT-calculated pK_{CO2} values versus the pK_{a1} and pK_{a2} for investigated primary and secondary amine molecules.

2.2 Results and discussion

2.2.1 Synthesis of alkoxides

Lithium phenoxide,[30] lithium catechoxide,[31] lithium trifluoroethoxide (TFE), lithium hexafluoropropoxide (HFP),[32] and tetramethylammonium phenoxide[33] were synthesized according to literature procedures. 2-nitrophenoxide, 2,6-dimethylphenoxide, 2,6-diisopropylphenoxide, and acetoate were synthesized using similar procedures as those above. These compounds are shown in Chart 1 with the pK_a of the relevant conjugate acid. Each isolated product was stored and manipulated under an inert N_2 atmosphere, as they degrade in the presence of oxygen.

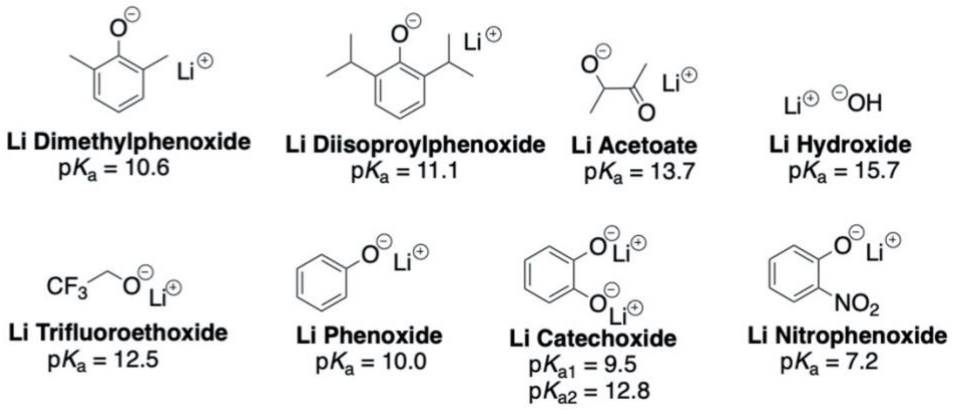

Chart 1. Initial alkoxides and phenoxides tested for CO_2 absorption. Names and pK_a of the conjugate acid is listed below each compound

2.2.2 Alkyl carbonate formation

First, alkoxides were tested for direct binding to CO_2 forming an alkyl carbonate, and to ensure they were not protonating in water. Infrared spectroscopy was used to detect the presence and absence of carbonate stretches for the alkoxides. The new peaks seen for Li trifluoroethoxide and Li catechoxide align with carbonate absorption after sparging with CO_2. Li phenoxide showed minor growth of a carbonate stretch after being sparged with CO_2 likely indicating weaker binding to CO_2 then the above alkoxides. Li HFP showed no evidence of alkyl carbonate formation (see Table 1 below).

	Expected Range (cm^{-1})	Li TFE	Li Catechoxide	Li Phenoxide	Li HFP
O-C-C	1060-1000	1033	1172	-	-
O-C-O	1280-1210	1201	1348	-	-
C=O	1800-1640	1649	1683	-	-
CO_2	2300	2360-2323	2360-2329	2358-2274	2360-2336

Table 1. The expected range for IR carbonate peaks, and the peaks shown for each alkoxide after being sparged with CO_2 are listed in wavenumbers cm^{-1}.

Mass spectrometry was used to detect formation of carbonate for Li TFE and Li HFP. Once CO_2 was introduced to a solution of Li TFE, a new peak at 144 m/z was observed in negative mode, corresponding to the expected trifluoroethyl carbonate anion peak. Conversely, Li HFP shows no indication of alkyl carbonate formation when exposed to CO_2.

^{1}H NMR and ^{13}C $\{^{1}H\}$ NMR spectroscopy were used to establish alkyl carbonate formation from peaks shifting in the spectra. In ^{13}C $\{^{1}H\}$ NMR, the carbonate peak in methanol-*d_4* appears at δ 159.98 for cesium carbonate and δ 169.36 for sodium carbonate, determined from commercially purchased carbonates. NMR spectra of Li TFE sparged with 100% CO_2 shows only one peak in the carbonate region at δ 160.10. To determine whether this carbonate peak relates to full conversion to the alkyl carbonate or to lithium carbonate, the precipitate from this reaction was collected. After 24 hours under benchtop conditions, the white power turned to a finer white solid. Analysis of this solid showed no Li TFE peaks present in the ^{1}H NMR spectrum, and a single peak at δ 167.92 visible by ^{13}C NMR. Thus, upon initial sparging of CO_2 Li TFE reacts to form lithium trifluoroethyl carbonate but if left under atmospheric conditions, it will degrade to lithium carbonate.

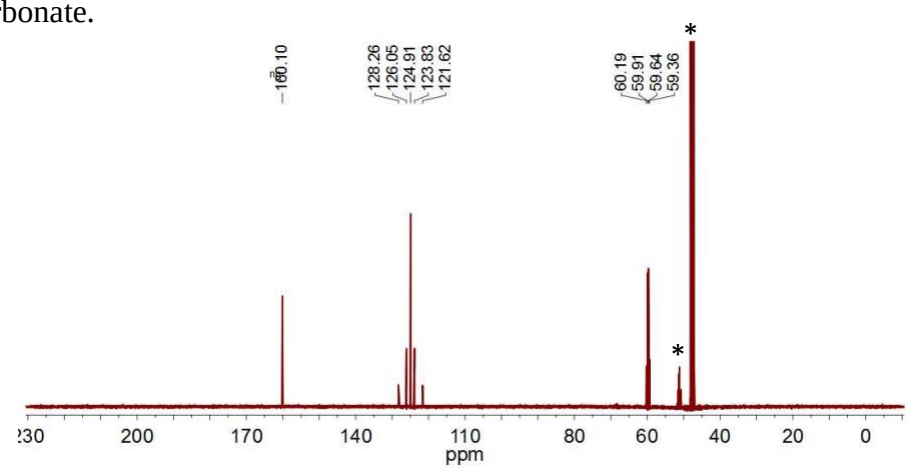

Figure 2. ^{13}C NMR of Li TFE sparged with CO_2 in CD_3OD with a T_1 of 25 sec. Peak at 160 ppm corresponds to the alkyl carbonate while 125 ppm corresponds to aqueous CO_2. '*' indicates peaks corresponding to impurities.

Out of four initial alkoxides selected to test alkyl carbonate formation, only Li trifluoroethoxide and Li catechoxide were found to form carbonates and with Li trifluoroethoxide forming the only mildly air stable complex. A potential explanation for the lack of carbonate formation using Li phenoxide and Li hexafluoropropoxide relates to the pK_a and nucleophilicity of the alcohols. Phenol (pK_a = 9.95) and hexafluoropropanol (pK_a = 9.3) both have a more basic pK_a than the two alkoxides that formed alkyl carbonates (catechol, pK_{a2} = 12.8; trifluoroethanol, pK_a = 12.5).[34] Since pK_a often correlates to nucleophilicity, these two conjugate bases are not nucleophilic enough to react and form an alkyl carbonate in significant amounts. Another reason for why Li phenoxide and Li hexafluoropropoxide do not form carbonates could be due to the binding strength between the alkoxide and lithium ion. The lithium ion may interact with alkoxy groups and prevent efficient CO_2 binding. By exchanging the counter ion for a much larger one, such as tetramethylammonium (TMA), we might be able to increase CO_2 capture.

2.2.3 EMAR

Since Li TFE demonstrated alkyl carbonate formation and was more air stable, methods for releasing the bound CO_2 were investigated. Hatton and coworkers developed an amine based electrochemical CO_2 capture system called electrochemically mediated amine regeneration (EMAR).[2,4–8] The initial step for EMAR remains the same as in amine thermal swing systems: amine capture of CO_2 through carbamate formation. The amine used in EMAR systems is ethylenediamine (EDA). The release step in EMAR makes use of preferential binding of EDA to copper. Electrochemically oxidizing copper releases Cu^{2+} into the system, EDA preferentially binds to Cu^{2+} ($K_{Cu} = 2.10 \times 10^{18}$) over CO_2 ($K_{CO2} = 4.90 \times 10^{4}$), which thus releases pure CO_2 for capture.[6] The copper is then plated out of the system by reduction at the cathode, regenerating

the EDA solution. Since alkoxides can also be used as ligands for metals, we predicted that a system similar to EMAR might be usable for alkoxides.

The preferential binding of Li TFE for CO_2 and various metals were tested using UV-visible spectroscopy. Spectra were taken for the aqueous metal solutions, aqueous metal solutions with CO_2 sparged through, aqueous metal solutions with Li TFE, Li TFE with CO_2, and aqueous metal solutions, Li TFE, and CO_2. The following metal salts were tested: Copper (II) acetate, copper (II) sulfate pentahydrate, iron (II) acetate, cobalt (II) acetylacetone, cobalt (II) tetrafluoroborate hexahydrate, nickel (II) tetrafluoroborate hexahydrate, zinc (II) tetrafluoroborate hexahydrate. While the spectra for Li TFE with the metal solutions showed binding – visibly seen as precipitate formation and color change – as soon as CO_2 was introduced the precipitate dissolved and a color change occurred (Figure 3). As such, preferential binding of alkoxide to metal was not observed for any metal as the alkoxide-metal bond is not seen through UV-vis when CO_2 is present.

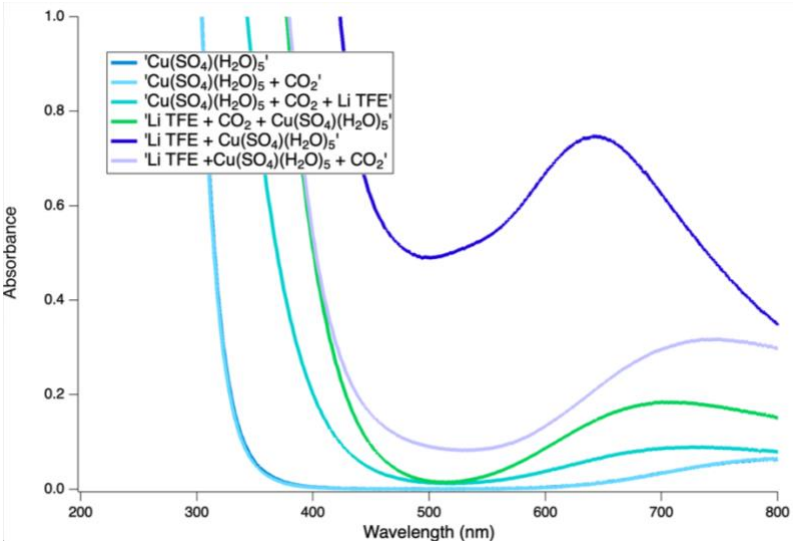

Figure 3. UV-vis spectra of Li TFE and copper (II) sulfate pentahydrate and it's reactivity with CO_2. When solely copper (II) sulfate is in the presence of CO_2 there is no reaction. The addition of Li TFE to this mixture results in a light green solution, from the original blue (λ_{max} = 796). However, if only Li TFE and copper (II) sulfate are combined, a dark blue precipitate forms (λ_{max} = 665). Even so, if this mixture is then sparged with CO_2 is also creates a the light green solution (λ_{max} = 736).

Alkoxides and alkyl carbonates are similar types of ligands. An alkoxide and an alkyl carbonate are both pi-donor ligands that bind to metal ions through an oxygen site. In addition,

their place on the spectrochemical series is quite similar. Comparing Li TFE with EDA as a ligand, EDA is a sigma-donor ligand and has a higher place on the spectrochemical series, meaning that it forms a stronger bond to metal ions than a carbamate would. In addition, EDA behaves as a bidentate ligand, further increasing its stability as a ligand through the chelate effect. All these factors contribute to allowing EDA to release CO_2 and preferentially bind to Cu^{2+}, while the differences in binding energies for alkoxides and alkyl carbonates are not distinct enough to promote preferential binding.

2.2.4 CO_2 absorption capacity of alkoxides

Even though using alkoxides in an EMAR-like system seems ineffective, alkoxides could be utilized in various other types of CO_2 capture systems, such as in electrochemical pH swings. To compare the binding efficiency of alkoxides and CO_2 to that of other capture agents like amines, the CO_2 absorption capacity for alkoxides was determined. CO_2 absorption capacity relates to how much direct inorganic carbon absorbs into solution, often expressed as moles of DIC per mole of capture agent or as gram of DIC per gram of capture agent. CO_2 absorption capacity not only measures the CO_2 absorbed through a reaction with alkoxides to form alkyl carbonates, but also aqueous CO_2, carbonate, and bicarbonate species.

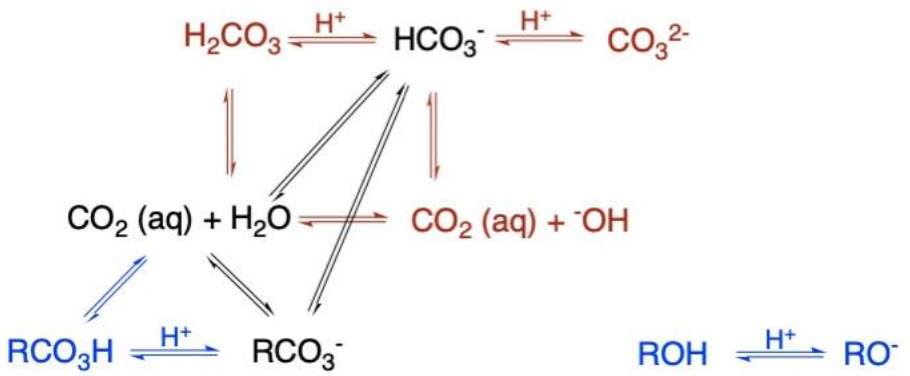

Scheme 1. equilibrium equations for alkoxide and CO_2 aqueous solutions.

CO_2 absorption capacity can be measured using various methods. The standard set up, however, remains the same: a CO_2 gas mixture of a known percentage (usually 10-15% CO_2) is

sparged through a system with a known amount of capture agent until the reaction is complete. The amount of CO_2 absorbed can be measured through a CO_2 gas analyzer, titrations, or from the change in mass of the solution. The most challenging part of all these systems is verifying when the reaction has reached equilibrium.[36,37] The method used was a modified version first presented by Puxty *et al*. that takes advantage of the mass change from CO_2 absorbing into solution.[37] Each alkoxide was tested a minimum of three times for accuracy.

Alkoxide (pK_a of conjugate acid)	**g_{CO2}/ $g_{alkoxide}$**	**n_{CO2} / $n_{alkoxide}$**
Li hydroxide (15.7)	0.72 ± 0.13	0.39 ± 0.07
Li acetoate (13.7)	0.11 ± 0.01	0.22 ± 0.03
Li catechoxide (12.8)	0.24 ± 0.05	0.66 ± 0.14
Li trifluoroethoxide (12.5)	0.18 ± 0.01	0.43 ± 0.03
Li 2,6-diisopropylphenoxide (11.1)	0.04 ± 0.02	0.16 ± 0.08
Li 2,6-dimethylphenoxide (10.6)	0.10 ± 0.04	0.30 ± 0.12
Li phenoxide (10.0)	0.07 ± 0.01	0.17 ± 0.03
Li 2-nitrophenoxide (7.2)	0.013 ± 0.004	0.04 ± 0.01

Table 2. Initial alkoxides and phenoxides tested for CO_2 absorption. Absorption capacity for each alkoxide is given as grams of CO_2 captured per gram of alkoxide and moles of CO_2 captured per mole of alkoxide.

In comparison, the standard amine used for CO_2 capture and concentration, MEA, has an absorption capacity of 0.56 mole CO_2 per mole MEA.[38] This is greater than expected, as an absorption capacity of 0.5 would be expected as the maximum for carbamate formation based on stoichiometry from equation 1. As such, an absorption capacity greater than 0.5 suggests that other pathways for CO_2 capture are occurring. Similarly, the largest absorption capacity expected for alkoxides would be 1, based on stoichiometry from equation 2. Even so, the highest absorption capacity observed is for Li catechoxide at 0.66 mole CO_2 per mole alkoxide (Table 2). The high absorption capacity could either be due to the presence of two sites for binding CO_2 on Li catechoxide or from one active binding site with a stabilization effect from the other alkoxy group. Comparing the data from the alkoxides to that of various amines, many amines

and alkoxides are all within the same range with each other. It should be noted that the molarity of the alkoxides solutions is 0.5 M while amines are mostly used at 30 wt% in water (~5 M for MEA).

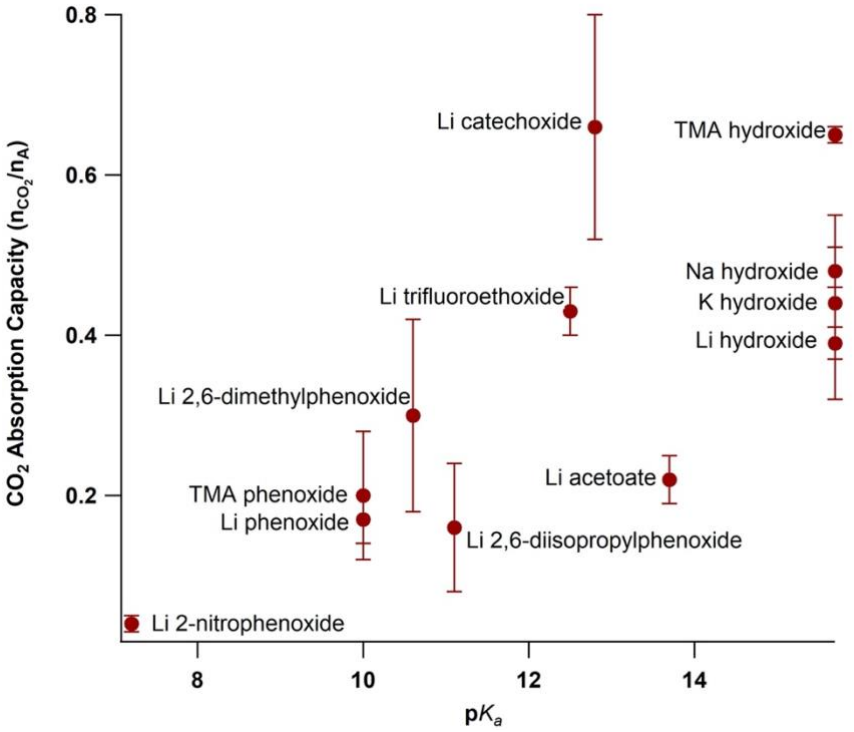

Figure 4. CO_2 absorption capacity of capture agent given as mole CO_2 absorbed per mole of capture agent used vs pK_a of the conjugate acid of the capture agent.

In addition, there is a mildly linear trend between pK_a and CO_2 absorption capacity, likely due to higher pK_a species corelating to greater nucleophilicity. If amines bind through the unprotonated amine, and pK_{a2} as the computational modeling predicts, amines have high binding constants. However, this high binding efficiency is inhibited through protonation of the amine by water, making it less effective for CO_2 capture, especially for direct air capture. As such, alkoxides offer a tradeoff of binding strength for water stability.

Phenoxides offer the potential for mild tunability to increase CO_2 absorption capacity. Examples of tunability are most evidently seen through comparing Li phenoxide, Li 2,6-dimethylphenoxide, and Li 2,6-diisopropylphenoxide. Computational modeling provided by our collaborators suggested that favorable CO_2 binding could be increased through addition of alkyl

groups at the 2 and 6 positions. These alkyl groups sterically force CO_2 to bind in the most stable conformation, thus increasing CO_2 binding. Li phenoxide has a CO_2 absorption capacity of 0.17 mole CO_2 per mole capture agent, where Li 2,6-dimethylphenoxide has an increased absorption capacity of 0.30, which supports the computational model. However, 2,6-diisopropylphenoxide shows decreased CO_2 absorption capacity of 0.16 mole CO_2 per mole capture agent. The decreased capture efficiency results from too much steric hindrance of CO_2, which appears to block the active site instead of forcing CO_2 into a favorable configuration.

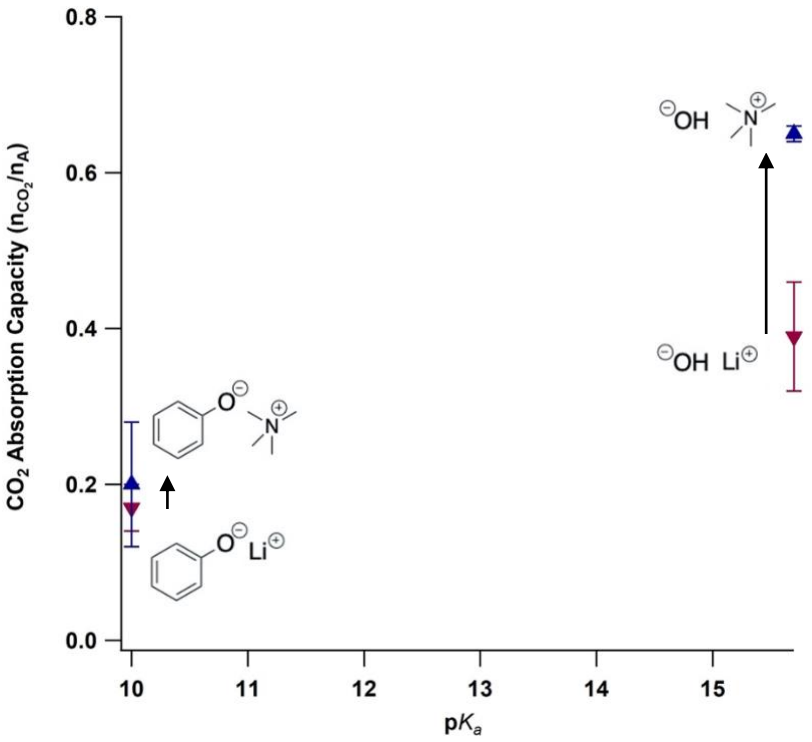

Figure 5. CO_2 absorption capacity vs pK_a for lithium phenoxide, lithium hydroxide, tetramethyl ammonium phenoxide, and tetramethyl ammonium hydroxide. The black arrows denote the difference in CO_2 absorption capacity for each salt by changing the counter cation from lithium to tetramethyl ammonium. As can be seen the change in absorption capacity is greater for hydroxide than it is for phenoxide.

Even with some tunable properties, alkoxides still do not reach their expected maximum absorption capacity of 1 mole CO_2 per mole capture agent. One reason for this could be that alkoxides are not strong enough nucleophiles to achieve this. However, it could also be that the lithium counter cation is affecting the capture efficiency from coordination to the active site. As such, it is possible that changing the counter cation could increase CO_2 absorption capacity.

Tetramethyl ammonium (TMA) was chosen as the counter cation to initially test this theory. TMA phenoxide was synthesized and tested for CO_2 absorption capacity, TMA hydroxide was purchased and tested as is. The absorption capacity for TMA phenoxide increased to 0.20 mole CO_2 per mole capture agent from 0.17, while TMA hydroxide increased to 0.65 mole CO_2 per mole capture agent from 0.39. This data indicates that the counter cation has an effect on the CO_2 binding affinity. However, the effect of the counter cation is not equivalent for these two alkoxides. The lesser effect of counter cations on phenoxides CO_2 capture efficiency could be due to the lower nucleophilicity for CO_2 that phenoxides inherently possess. Thus, if the capture ability of phenoxides is low to begin with, the counter cation will not affect the CO_2 absorption capacity drastically.

2.2.5 Cation effects on CO_2 absorption capacity of hydroxides

Since counter cations affect CO_2 absorption capacity, optimizing CO_2 capture through counter cation choice was studied. Because hydroxides with various counter cations are commercially available, hydroxide was used as the standard capture agent for this investigation. Hydroxides are a good model for CO_2 absorption capacity since they limit the forms of CO_2 in water to aqueous carbon dioxide, carbonate, bicarbonate, or carbonic acid.

The data shows that cesium hydroxide has the highest CO_2 absorption capacity. Studies involving electrochemical reduction of CO_2 have also shown cation sensitivity, often with 1-3 orders of magnitude difference in activity between Li^+ and Cs^+ containing electrolytes.[39,40] While these systems postulate the electrolyte is able to aid in CO_2 reduction through hydrolysis of the cations onto the electrode surface or through electrostatic interactions with the electric dipole of specific absorbates, they still offer insight into how cations interact with CO_2 and carbonate species. In particular, the hydrated cation models show that Cs^+ has a much smaller radius than

Li^+ which can lead to higher local concentrations of Cs^+.[40] In this manner, Cs^+ may be able to stabilize bicarbonate more effectively in solution, thus leading to more CO_2 absorption.

Another method for predicting effectiveness of CO_2 absorption offered by cations is found by examining the activity of each hydroxide instead of the pK_a. Activity can be inferred by pH of the capture agent (higher pH indicating stronger activity).[41] Looking at Figure 6, a higher starting pH for the 0.5 M hydroxide solutions tends to correlate with a higher CO_2 absorption capacity. Even so, cesium remains an outlier in this instance as well.

The size of the counter cations does not show a trend for CO_2 capture preference. Theoretically, a counter cation's optimal size would be large enough to not coordinate too extensively with the alkoxy group, but small enough to not sterically hinder access to the bonding site. By comparing CO_2 absorption capacity and the radii of the solid-state cation, we had hoped to see a bell-shaped curve to match the above hypothesis. In such a way, the two center cations, Cs^+ and TMA^+, do show the highest absorption capacity. However, using the calculated hydrated ionic radii for these counter cations indicated that in aqueous solution, the radii are not that distinguishable. As such, this metric might not be the best for determining a trend for the ideal counter cations for CO_2 capture.

Counter cation	**g_{CO2}/g_{OH}**	**n_{CO2}/n_{OH}**	**Crystal radii (Å)[a]**	**Hydrated radii (Å)[a]**	**Initial pH**
Li^+	0.72 ± 0.13	0.39 ± 0.07	0.60	3.82	13.30
Na^+	0.53 ± 0.08	0.48 ± 0.07	0.95	3.58	13.33
K^+	0.33 ± 0.03	0.44 ± 0.07	1.33	3.31	13.58
Cs^+	0.25 ± 0.02	0.84 ± 0.05	1.69	3.29	13.90
TMA^+	0.320 ± 0.006	0.65 ± 0.01	3.47	3.67	14.50
TEA^+	0.17 ± 0.01	0.58 ± 0.04	4.00	4.00	13.84
TPA^+	0.10 ± 0.02	0.46 ± 0.07	4.52	4.52	13.25
TBA^+	0.09 ± 0.01	0.54 ± 0.06	4.94	4.94	14.31

[a] radii taken from Nightingale [47]

Tabel 3. The CO_2 absorption capacity was tested for hydroxide with the various counter cations given. The CO_2 absorption capacity is given as grams of CO_2 captured per gram of hydroxide and mole of CO_2 captured per mole of hydroxide. Also given are both the crystalline and hydrated ionic radii for each counter cation. Lastly, the starting pH for each 0.5 M aqueous solution is listed.

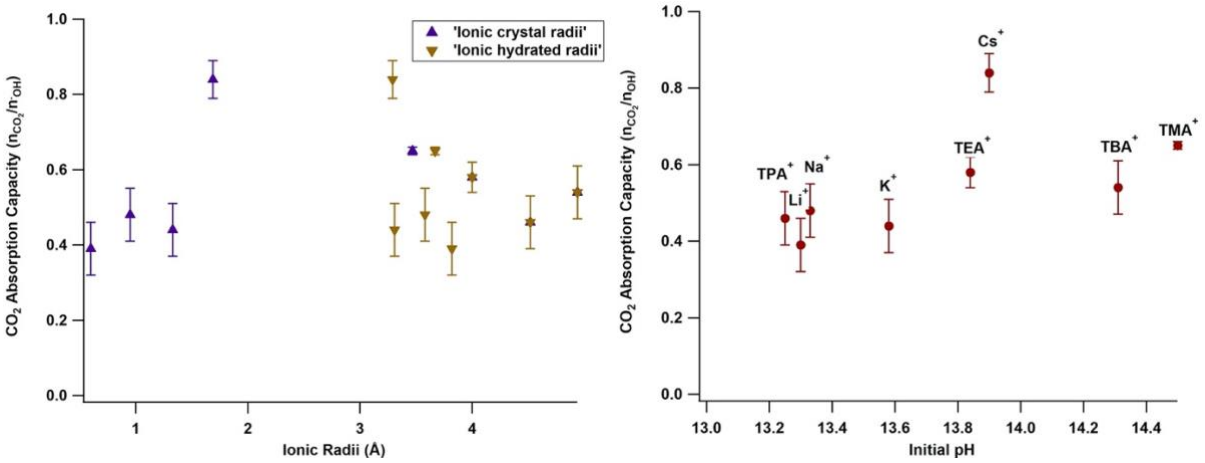

Figure 6. (left) CO_2 absorption capacity of hydroxide with different counter cations vs ionic radii. The purple triangle denotes the radii based on crystalline cations and the brown reverse triangle is the radii calculated hydrated radii. (right) CO_2 absorption capacity of hydroxide vs the initial pH of each 10 mL 0.5 M solution.

3. CO_2 capture and concentration using photoacids

3.1 Background

Photoacids offer an intriguing alternative route for CO_2 capture since they can be used to generate localized pH swings. Photoacids are organic or inorganic Brønsted acids which have a ground state pK_a, and upon photoexcitation, become stronger acids with an excited state pK_a (pK_a*).[42–44] Due to this distinctive property, photoacids could be used in a system similar to electrochemical pH swings. In addition, certain photoacids have already been found that preferentially protonate bicarbonate over water, as shown in a study finding the pK_a of carbonic acid using 6-hydroxy-1-sulfonate pyrene.[45] Thus, a CO_2 capture and concentration system based on photoacids should be feasible.

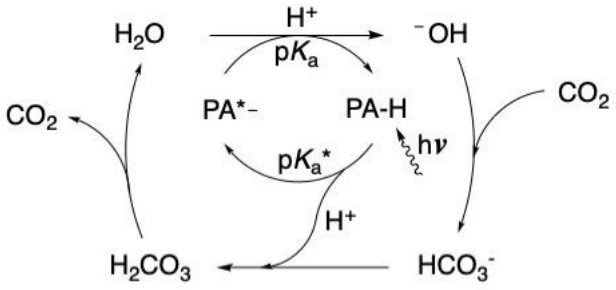

Figure 7. pH swing cycle of a photoacid molecule, PA, mediating CO_2 capture via OH^- and H^+.

A general scheme for CO_2 capture using photoacids can been seen in Figure 7. CO_2 is first absorbed into a high pH solution, and then the photoacid in solution is activated by light, thereby releasing a proton due to the lower pK_a of the excited state. This creates a localized pH drop, causing the release of CO_2 due to the lower solubility of CO_2 in more acidic solutions. The photoacids chosen for this process require three key characteristics: 1) a large difference between pK_a and pK_a* (change of 7 units), 2) high solubility in water, and 3) an excitation period that is long enough to change the pH of the solution, but short enough to release CO_2 in a timely manner (on the nanosecond scale). The initial photoacid selected for testing was 1-naphthol-4-sulfonate (1N4S), which has a pK_a of 8.27 and pK_a* of -0.1, good solubility for a photoacid, and excitation lifetime of 2.2 x 10^{10} s^{-1}.[42,46]

3.2 Results and discussion

The first step towards designing a CO_2 capture and concentration system using photoacids as a proton source is optimizing absorption of CO_2 into solution. Since CO_2 reacts with hydroxide to form bicarbonate, the more hydroxide in solution (and thus the more alkaline the solution) the more CO_2 can be absorbed. Gas absorption was achieved by sparging a basic solution (pH of 10-12) of 150 µM 1N4S with CO_2 for roughly one hour to ensure saturation and relative equilibrium of dissolved CO_2 and bicarbonate in solution. At the end of this process, the pH of the solution was measured to be 7. The next step is excitation of the photoacid in solution. The photoacid selected for excitation studies, 1N4S, has an electronic absorbance of λ_{max} = 300

nm (ε = 6900 cm^{-1} M^{-1}). The pK_a and pK_a* of 1N4S was previously reported as pK_a = 8.27 and pK_a* = -0.1.[42]

To investigate CO_2 release during photoacid excitation, the first experiments were completed in a closed system. During the 3-hour excitation of 1N4S using a UV-vis spectrometer, the atmosphere of the system reached 100% CO_2, thus showing that CO_2 was released. Control experiments in the absence of photoacid or photoexcitation indicate that the excited photoacid is necessary for CO_2 release (Figure 8). However, this system does not allow for the quantification of CO_2 released. Thus, an open system was created to test photoacid driven CO_2 release quantitatively.

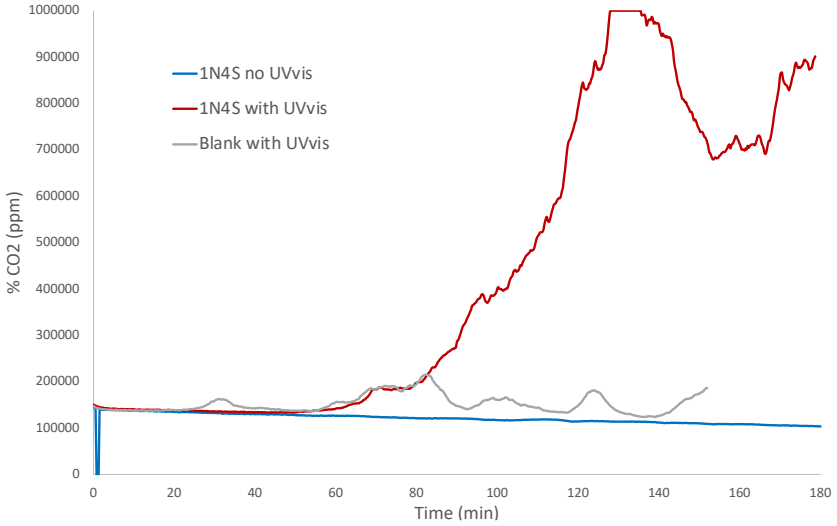

Figure 8. Closed system of CO_2 capture using 150 µM 1N4S in aqueous solution. Percentage of CO_2 measured in headspace (ppm) over time for when photoacid and no light source present, photoacid with light excitation, and no photoacid with light excitation.

For the open system, N_2 was circulated through the solution at a flow rate of ~5 mL/min to monitor CO_2 release after excitation. Due to the change in atmosphere from 10% CO_2 to 100% N_2, some CO_2 is released for equilibrium at the beginning of each run before excitation begins. In the absence of photoacid, the only CO_2 release is due to the equilibrium shifting from the change in atmosphere, showing that the presence of the photoacid is necessary for further CO_2 release. However, when no photoexcitation is present there is still a large volume of CO_2

released (blue trace in Figure 9). This could be caused by the comparatively slow flow rate of N_2, which varies dramatically over time and can make the output of CO_2 seem larger than in actuality.

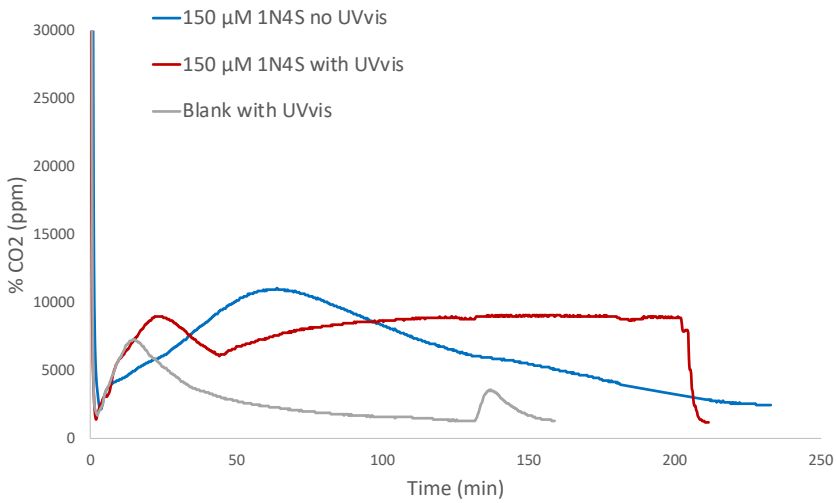

Figure 9. Open system of CO_2 capture using 150 µM 1N4S in aqueous solution. Percentage of CO_2 (ppm) measured at outlet over time for when photoacid and no light source present, photoacid with light excitation, and no photoacid with light excitation.

Since the open system for photoacid CO_2 capture and release has a known flow rate and percentage of CO_2 exiting the system, the total amount of CO_2 absorbed and released can be quantified. By integrating under the curve for percent CO_2 during the absorbance and release steps, an estimate of the amount of CO_2 that is absorbed and released can be found. In one run, 11.1 mL of CO_2 was absorbed into solution to create a concentration of 0.15M CO_2. The amount of CO_2 emitted for this run was calculated to be 12.4 mL. Errors in this measurement are likely due to the setup of the system as currently there is only a CO_2 sensor at the outlet. If an additional CO_2 sensor were included at the inlet as well, the baseline for CO_2 in the system would be known and would not have to be estimated (as was done in the above calculations).

4. Conclusions

This work sought to explore new methods for CO_2 capture other than amine thermal swing systems. Both direct and indirect capture were studied using alkoxides and the unique pK_as of photoacids.

Alkoxides were used as a mode of direct carbon capture. Alkoxides were found to capture CO_2 from simulated flue gas (10% CO_2, 90% N_2) with CO_2 absorption capacities comparable to many amine capture agents. Even so, the CO_2 absorption capacity was lower than anticipated. This result may be due to cation effects which were studied in more depth using hydroxides with various counter cations. We found that exchanging the cation led to significant changes in CO_2 absorption capacity, with a range of 0.39 to 0.84 mole CO_2 captured per mole of hydroxide. Understanding the properties that lead to greater CO_2 absorption capacity for alkoxides will lead to more efficient CO_2 capture and concentration systems. In cases like pH swings, where CO_2 is often first absorbed into solution through sodium hydroxide, using a capture agent that can absorb greater amounts of CO_2 from the waste stream would improve the process.

Indirect carbon capture and concentration was probed using photoacids. Since photoacids have two distinct pK_as for the ground state and the excited state, creating localized pH swings using photoexcitation offers a new CO_2 capture and concentration using photons. Preliminary works suggests that the photoacid 1N4S can successfully release CO_2 from solution upon excitation. However, at this time, more work is needed of the system design. In particular, increasing the intensity of the excitation source should greatly improve measurements.

5. Experimental

Synthesis and manipulation of compounds were carried out in open air unless otherwise mentioned. For air- and moisture-sensitive procedures, manipulations were carried out in a glovebox or using standard Schlenk techniques under inert atmosphere of nitrogen. Pentane and toluene used during inert atmosphere synthesis and/or manipulations was degassed by sparging with argon and dried by passing through columns of neutral alumina or molecular sieves. Water used during inert atmosphere synthesis and/or manipulations was degassed using active vacuum for several hours. All deuterated solvents were purchased from Cambridge Isotope Laboratories, Inc. Deuterated methanol, DMSO, benzene, and water were degassed and methanol and DMSO stored over activated 3 Å molecular sieves prior to use. All solvents and reagents were purchased from commercial vendors and used without further purification unless otherwise noted. The compounds in Figure 6a are synthesized using two routes:

Synthesis using LiOH: This synthetic route was used for deprotonation of trifluoroethanol, hexafluoropropanol, 2-nitrophenol, and 2,6-dimethylphenol. Under an N_2 atmosphere, 25 mmol of alcohol was combined with 25 mmol of lithium hydroxide in 20 mL dry methanol. The reaction was refluxed overnight then dried under vacuum to give solid.

Synthesis using n-butyl lithium: This synthetic route was used to deprotonate phenol, 2,6-diisopropylphenol, and catechol. Alcohols were first stirred with toluene for an hour, then dried under vacuum to remove excess water. Under an N_2 atmosphere with 50 mL dried pentane from the solvent system and 25 mmol of dried alcohol, 25 mmol (or 50 mmol for catechol) 1.6 M n-butyl lithium in hexane was added dropwise at -78°C. The mixture was stirred at -78°C for one hour, and then stirred for an additional 24 hours at room temperature. Solvent was removed under reduced pressure to leave a colorless solid.

NMR spectroscopy was used to confirm the identity and purity of the synthesized compounds. ^{1}H NMR spectroscopy was performed on a 500MHz Bruker Avance GN500 with a BBO probe or on a 500 MHz Bruker DRX 500 spectrometer with a TCI cryoprobe. $^{13}C\{^{1}H\}$ NMR spectra were recorded on a 500MHz Bruker DRX 500 fitted with a TCI cryoprobe. All NMR spectra were acquired at room temperature and referenced to residual ^{1}H or ^{13}C resonances of the deuterated solvent (^{1}H: CD_3OD, δ 3.31; D_2O, δ 4.79; DMSO-D_6, δ 2.50; C_6D_6, δ 7.16) (^{13}C: CD_3OD, δ 49.00; D_2O, δ -; DMSO-D_6, δ 39.52).

Lithium phenoxide (C1)

^{1}H NMR (500 MHz, DMSO) δ 6.82 (t, *J* = 7.0 Hz, 2H), 6.37 (s, 1H), 6.10 (s, 1H); $^{13}C\{^{1}H\}$ NMR (126 MHz, DMSO) δ 170.16, 128.88, 120.03, 109.97.

Lithium 2,6-dimethylphenoxide (C2)

^{1}H NMR (500 MHz, C_6D_6) δ 7.04 (d, *J* = 6.9 Hz, 2H), 6.71 (t, *J* = 7.3 Hz, 1H), 2.15 (s, 6H); $^{13}C\{^{1}H\}$ NMR (126 MHz, D_2O) δ 163.46, 128.21, 127.04, 113.61, 17.34.

Lithium 2,6-diisopropylphenoxide (C3)

^{1}H NMR (500 MHz, D_2O) δ 7.03 (d, *J* = 7.4 Hz, 2H), 6.60 (t, *J* = 7.4 Hz, 1H), 3.37 (q, *J* = 6.9 Hz, 2H), 1.13 (d, *J* = 6.9 Hz, 12 H); $^{13}C\{^{1}H\}$ NMR (126 MHz, D_2O) δ 160.14, 138.31, 122.81, 114.19, 25.82, 23.00.

Lithium catechoxide (C4)

^{1}H NMR (500 MHz, DMSO) δ 6.27 (s, 2H), 5.94 (s, 2H); $^{13}C\{^{1}H\}$ NMR (126 MHz, D_2O) δ 161.56, 116.33, 112,74.

Lithium 2-nitrophenoxide (C5)

^{1}H NMR (500 MHz, D_2O) δ 7.89 (d, *J* = 8.4 Hz, 1H), 7.36 (t, *J* = 7.7 Hz, 1H), 6.79 (d, *J* = 8.7 Hz, 1H), 6.51 (t, *J* = 7.6 Hz, 1H); ^{13}C{^{1}H} NMR (126 MHz, D_2O) δ 165.77, 137.50, 136.06, 126.42, 125.43, 113.06.

Lithium 2,2,2-trifluoroethoxide (C6)

^{1}H NMR (500 MHz, CD_3OD) δ 3.86 (q, *J* = 9.2 Hz, 2H); ^{13}C{^{1}H} NMR (126 MHz, CD_3OD) δ 129.35, 127.19, 124.93, 122.75, 61.83, 61.56, 61.30, 61.06; ^{19}F NMR (565 MHz, D_2O) δ -76.44.

CO_2 Absorption Capacity Methods: The CO_2 absorption capacity measurements were made following the procedure previously described by Puxty *et al*. 10 mL 0.5 M alkoxide solution was placed in weighed 20 mL vial with septum screw top and stir bar (below). First, the mass change due to evaporation was recorded by placing the vial in 40 °C bath and sparging with N_2. The inlet needle was never placed directly into solution, only the headspace. The change in mass was measured 8 times over a period of 20 minutes. Next, the gas inlet was changed to 10% CO_2. The change in mass was measured every minute for the first 10 minutes, and then every 5 minutes for an hour. The flow rate of the inlet gas does not matter much as long as it is consistent from the evaporation to the absorption test. If the flow rate changes between these two experiments, the trendline for the evaporation will no longer be accurate and thus the absorption capacity will not be accurate. The change in flow rate is the most common cause of error for this data. To determine the overall CO_2 absorption, the mass change due to evaporation alone was subtracted from mass change when 10% CO_2 was used to give the total mass gained due to CO_2 absorption. The value for CO_2 absorption capacity was determined from where the final absorption curve plateaus. The value for total mass (in grams) at the plateau is then divided by the mass of the alkoxide dissolved in solution, giving the value of grams of CO_2 captured per grams of alkoxide. To change this to moles of CO_2 captured per mole of alkoxide, the value is divided by the molar

mass of CO_2 and multiplied by the molar mass of the alkoxide. This method was validated against the original data from Puxty *et al.* using ethylenediamine as the standard.

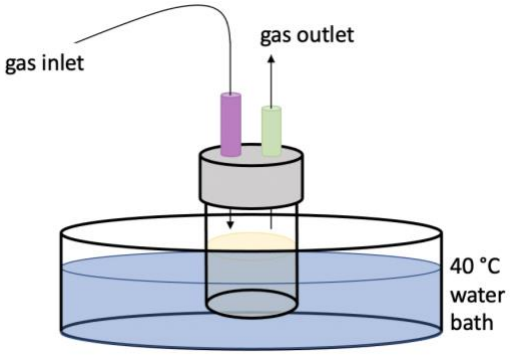

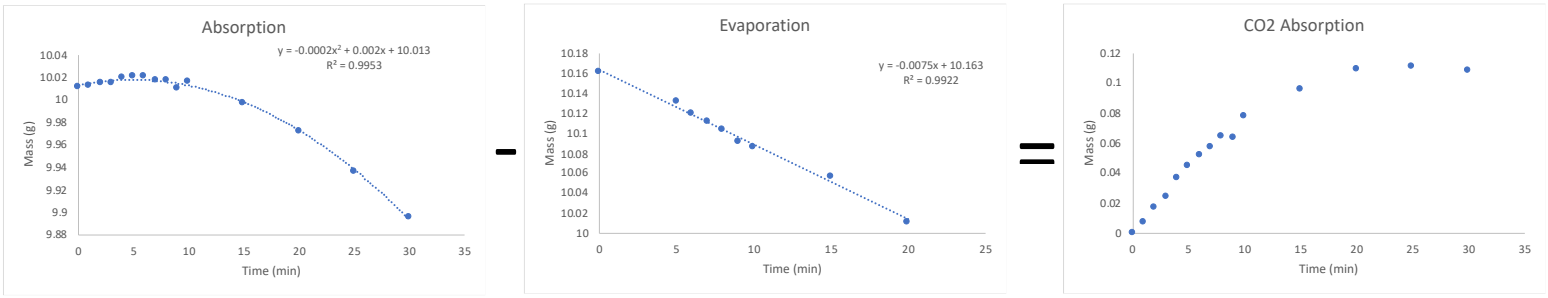

Photoacid System Methods: From 5 mM stock solution of 1-naphthol-4-sulfonate (1N4S), a basic solution of 150 µM 1N4S is made. The pH of the solution is then measured using a pH probe (pH between 10-12). Next 3 mL of solution is transferred to cuvette with septum lid. The solution is next sparged with 10% CO_2 at a flow rate of ~5 mL/min for 1 hour while the CO_2 sensor measures CO_2 percentage at the outlet. Next the system is sparged with 100% N_2 for 30 minutes to get a baseline for CO_2. The photoacid is then excited using UV-vis light at 300 nm for about 3 hours measuring any change of CO_2 at the outlet. By also measuring the percentage of CO_2 at the inlet, the total volume of CO_2 captured and released in this process can be determined from integrating the difference between the inlet and outlet CO_2 percentage.

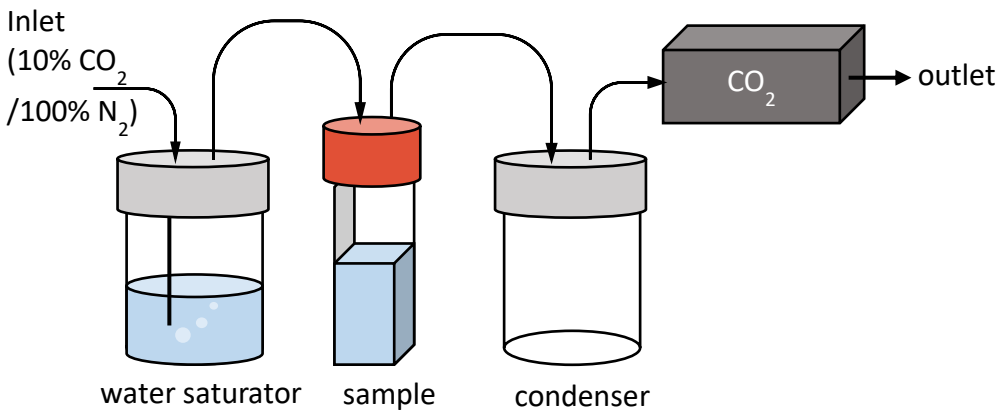

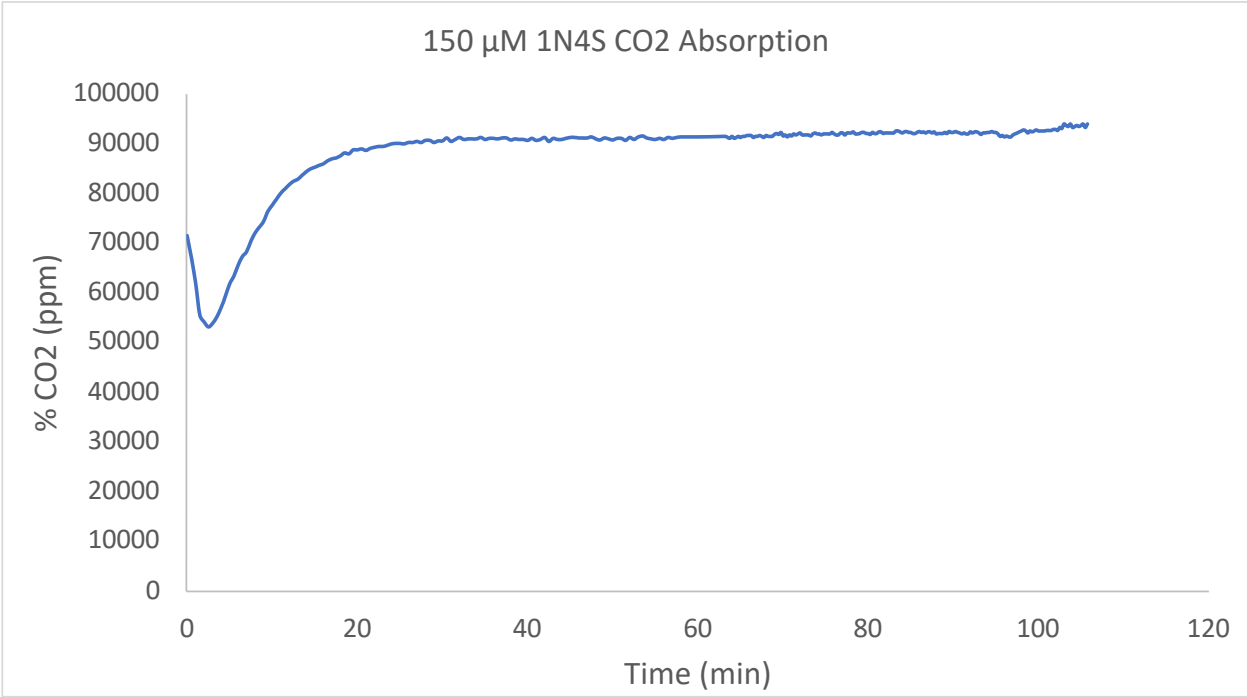

Sample CO_2 absorption for the photoacid system. 10% CO_2 was sparged through the system and monitored at the outlet with a CO_2 sensor. The dip at the beginning of the graph shows that the %CO_2 at the outlet is lower since CO_2 is being absorbed into solution. This reaction usually reaches equilibrium after 30-60 minutes.

6. References

(1) IEA. Global Energy Review: CO2 Emissions in 2021. Paris 2021.

(2) Fasihi, M.; Efimova, O.; Breyer, C. Techno-Economic Assessment of CO 2 Direct Air Capture Plants. *J. Clean. Prod.* **2019**, *224*, 957–980. https://doi.org/10.1016/j.jclepro.2019.03.086.

(3) Mondal, M. K.; Balsora, H. K.; Varshney, P. Progress and Trends in CO2 Capture/Separation Technologies: A Review. *Energy* **2012**. https://doi.org/10.1016/j.energy.2012.08.006.

(4) Sayari, A.; Belmabkhout, Y.; Serna-Guerrero, R. Flue Gas Treatment via CO2 Adsorption. *Chem. Eng. J.* **2011**, *171* (3), 760–774. https://doi.org/10.1016/j.cej.2011.02.007.

(5) Mondal, M. K.; Balsora, H. K.; Varshney, P. Progress and Trends in CO2 Capture/Separation Technologies: A Review. *Energy* **2012**, *46* (1), 431–441. https://doi.org/10.1016/j.energy.2012.08.006.

(6) Shaw, R. A.; Hatton, T. A. Electrochemical CO2 Capture Thermodynamics. *Int. J. Greenh. Gas Control* **2020**, *95*. https://doi.org/10.1016/j.ijggc.2019.102878.

(7) Svendsen, H. F.; Hessen, E. T.; Mejdell, T. Carbon Dioxide Capture by Absorption, Challenges and Possibilities. *Chem. Eng. J.* **2011**, *171* (3), 718–724. https://doi.org/10.1016/j.cej.2011.01.014.

(8) Leung, D. Y. C.; Caramanna, G.; Maroto-Valer, M. M. An Overview of Current Status of Carbon Dioxide Capture and Storage Technologies. *Renewable and Sustainable Energy Reviews*. 2014. https://doi.org/10.1016/j.rser.2014.07.093.

(9) Wang, M.; Herzog, H. J.; Hatton, A. T. CO2 Capture Using Electrochemically Mediated Amine Regeneration. *Ind. Eng. Chem. Reserach* **2020**, *59*, 7087–7096.

(10) Wang, M.; Hariharan, S.; Shaw, R.; Hatton, A. T. Energetics of Electrochemically Mediated Amine Regeneration Process for Flue Gas CO2 Capture. *Int. J. Greenh. Gas Control* **2018**.

(11) Wang, M.; Rahimi, M.; Kumar, A.; Hariharan, S.; Choi, W.; Hatton, T. A. Flue Gas CO2 Capture via Electrochemically Mediated Amine Regeneration: System Design and Performance. *Appl. Energy* **2019**, *255*. https://doi.org/10.1016/j.apenergy.2019.113879.

(12) Stern, M. C.; Simeon, F.; Herzog, H.; Hatton, T. A. Post-Combustion Carbon Dioxide Capture Using Electrochemically Mediated Amine Regeneration. *Energy Environ. Sci.* **2013**, *6* (8), 2505–2517. https://doi.org/10.1039/c3ee41165f.

(13) Stern, M. C.; Alan Hatton, T. Bench-Scale Demonstration of CO2 Capture with Electrochemically-Mediated Amine Regeneration. *RSC Adv.* **2014**, *4* (12), 5906–5914. https://doi.org/10.1039/c3ra46774k.

(14) Renfrew, S. E.; Starr, D. E.; Strasser, P. Electrochemical Approaches toward CO2Capture and Concentration. *ACS Catal.* **2020**, *10* (21), 13058–13074. https://doi.org/10.1021/acscatal.0c03639.

(15) Jin, S.; Wu, M.; Gordon, R. G.; Aziz, M. J.; Kwabi, D. G. PH Swing Cycle for CO2capture Electrochemically Driven through Proton-Coupled Electron Transfer. *Energy Environ. Sci.* **2020**, *13* (10), 3706–3722. https://doi.org/10.1039/d0ee01834a.

(16) Sharifian, R.; Wagterveld, R. M.; Digdaya, I. A.; Xiang, C.; Vermaas, D. A. Electrochemical Carbon Dioxide Capture to Close the Carbon Cycle. *Energy Environ. Sci.* **2021**. https://doi.org/10.1039/d0ee03382k.

(17) Rheinhardt, J. H.; Singh, P.; Tarakeshwar, P.; Buttry, D. A. Electrochemical Capture and Release of Carbon Dioxide. *ACS Energy Lett.* **2017**, *2* (2), 454–461. https://doi.org/10.1021/acsenergylett.6b00608.
(18) Scovazzo, P.; Poshusta, J.; DuBois, D.; Koval, C.; Noble, R. Electrochemical Separation and Concentration of <1% Carbon Dioxide from Nitrogen. *J. Electrochem. Soc.* **2003**, *150* (5), D91. https://doi.org/10.1149/1.1566962.
(19) Chang, R.; Kim, S.; Lee, S.; Choi, S.; Kim, M.; Park, Y. Calcium Carbonate Precipitation for CO 2 Storage and Utilization: A Review of the Carbonate Crystallization and Polymorphism. *Frontiers in Energy Research*. Frontiers Media S.A. July 10, 2017. https://doi.org/10.3389/fenrg.2017.00017.
(20) Li, H.; Li, L.; Lin, R.-B.; Zhou, W.; Zhang, Z.; Xiang, S.; Chen, B. Porous Metal-Organic Frameworks for Gas Storage and Separation: Status and Challenges. *EnergyChem* **2019**, *1* (1), 100006. https://doi.org/10.1016/j.enchem.2019.100006.
(21) Conway, W.; Wang, X.; Fernandes, D.; Burns, R.; Lawrance, G.; Puxty, G.; Maeder, M. Toward Rational Design of Amine Solutions for PCC Applications: The Kinetics of the Reaction of CO2(Aq) with Cyclic and Secondary Amines in Aqueous Solution. *Environ. Sci. Technol.* **2012**, *46* (13), 7422–7429. https://doi.org/10.1021/es300541t.
(22) McCann, N.; Phan, D.; Wang, X.; Conway, W.; Burns, R.; Attalla, M.; Puxty, G.; Maeder, M. Kinetics and Mechanism of Carbamate Formation from CO2(Aq), Carbonate Species, and Monoethanolamine in Aqueous Solution. *J. Phys. Chem. A* **2009**, *113* (17), 5022–5029. https://doi.org/10.1021/jp810564z.
(23) Darunte, L. A.; Oetomo, A. D.; Walton, K. S.; Sholl, D. S.; Jones, C. W. Direct Air Capture of CO2 Using Amine Functionalized MIL-101(Cr). *ACS Sustain. Chem. Eng.* **2016**, *4* (10), 5761–5768. https://doi.org/10.1021/acssuschemeng.6b01692.
(24) Kim, E. J.; Siegelman, R. L.; Jiang, H. Z. H.; Forse, A. C.; Lee, J. H.; Martell, J. D.; Milner, P. J.; Falkowski, J. M.; Neaton, J. B.; Reimer, J. A.; Weston, S. C.; Long, J. R. Cooperative Carbon Capture and Steam Regeneration with Tetraamine-Appended Metal-Organic Frameworks. *Science (80-.).* **2020**, *369* (6502), 392–396. https://doi.org/10.1126/science.abb3976.
(25) Anyanwu, J. T.; Wang, Y.; Yang, R. T. CO2 Capture (Including Direct Air Capture) and Natural Gas Desulfurization of Amine-Grafted Hierarchical Bimodal Silica. *Chem. Eng. J.* **2022**, *427* (May 2021), 131561. https://doi.org/10.1016/j.cej.2021.131561.
(26) Gabsi, W.; Boubaker, T.; Goumont, R. Nucleophilicities of Para-Substituted Phenoxide Ions in Water and Correlation Analysis. *Int. J. Chem. Kinet.* **2014**, *46* (12), 711–717. https://doi.org/10.1002/kin.20846.
(27) Bruice, T. C.; Fife, T. H.; Bruno, J. J.; Brandon, N. E. Hydroxyl Group Catalysis. II. The Reactivity of the Hydroxyl Group of Serine. The Nucleophilicity of Alcohols and the Ease of Hydrolysis of Their Acetyl Esters as Related to Their PKa. *Biochemistry* **1962**, *1* (1), 7–12. https://doi.org/10.1021/bi00907a002.
(28) Zhang, Z.; Kummeth, A. L.; Yang, J. Y.; Alexandrova, A. N. Inverse Molecular Design of Alkoxides and Phenoxides for Aqueous Direct Air Capture of CO2. *Proc. Natl. Acad. Sci. U. S. A.* **2022**, *119* (25), 1–11. https://doi.org/10.1073/pnas.2123496119.
(29) Bernhardsen, I. M.; Knuutila, H. K. A Review of Potential Amine Solvents for CO2 Absorption Process: Absorption Capacity, Cyclic Capacity and PKa. *International Journal of Greenhouse Gas Control*. 2017. https://doi.org/10.1016/j.ijggc.2017.03.021.
(30) Den Besten, R.; Harder, S.; Brandsma, L. *A Method for the Determination of the Degree*

of Association of Organolithium Compounds in Liquid Ammonia; Elsevier Sequoia S.A, 1990.
(31) Bayliff, A. E.; Bryce, M. R.; Chambers, R. D. *Polyhalogenoheterocyclic Compounds. Part 38.' Reactions of Fluorinated-Alkenes and-Cycloalkenes with Difunctional Nucleophiles*; 1987.
(32) Yang, Z. Z.; He, L. N. Efficient CO2 Capture by Tertiary Amine-Functionalized Ionic Liquids through Li,+-Stabilized Zwitterionic Adduct Formation. *Beilstein J. Org. Chem.* **2014**, *10*, 1959–1966. https://doi.org/10.3762/bjoc.10.204.
(33) Cismesia, M. A.; Ryan, S. J.; Bland, D. C.; Sanford, M. S. Multiple Approaches to the in Situ Generation of Anhydrous Tetraalkylammonium Fluoride Salts for SNAr Fluorination Reactions. *J. Org. Chem.* **2017**, *82* (10), 5020–5026. https://doi.org/10.1021/acs.joc.7b00481.
(34) Ripin, D. H.; Evans, D. A. PKa Table. https://doi.org/10.5.
(35) Liu, Y.; Ye, H. Z.; Diederichsen, K. M.; Van Voorhis, T.; Hatton, T. A. Electrochemically Mediated Carbon Dioxide Separation with Quinone Chemistry in Salt-Concentrated Aqueous Media. *Nat. Commun.* **2020**, *11* (1), 1–11. https://doi.org/10.1038/s41467-020-16150-7.
(36) Matin, N. S.; Remias, J. E.; NEathery, J. K.; Liu, K. Facile Method for Determination of Amine Speciation in CO2 Capture Solutions.Pdf. *Ind. Eng. Chem. Reserach Eng. Chem. Res.* **2012**, *51*, 6613–6618. https://doi.org/dx.doi.org/10.1021/ie300230.
(37) Puxty, G.; Rowland, R.; Allport, A.; Yang, Q.; Bown, M.; Burns, R.; Maeder, M.; Attalla, M. Carbon Dioxide Postcombustion Capture: A Novel Screening Study of the Carbon Dioxide Absorption Performance of 76 Amines. *Environ. Sci. Technol.* **2009**, *43* (16), 6427–6433. https://doi.org/10.1021/es901376a.
(38) Bernhardsen, I. M.; Knuutila, H. K. A Review of Potential Amine Solvents for CO2 Absorption Process: Absorption Capacity, Cyclic Capacity and PKa. *International Journal of Greenhouse Gas Control*. Elsevier Ltd 2017, pp 27–48. https://doi.org/10.1016/j.ijggc.2017.03.021.
(39) Moura de Salles Pupo, M.; Kortlever, R. Electrolyte Effects on the Electrochemical Reduction of CO2. *ChemPhysChem* **2019**, *20* (22), 2926–2935. https://doi.org/10.1002/cphc.201900680.
(40) Ringe, S.; Clark, E. L.; Resasco, J.; Walton, A.; Seger, B.; Bell, A. T.; Chan, K. Understanding Cation Effects in Electrochemical CO2 Reduction. *Energy Environ. Sci.* **2019**, *12* (10), 3001–3014. https://doi.org/10.1039/c9ee01341e.
(41) McCarty, C. G.; Vitz, E. PH Paradoxes: Demonstrating That It Is Not True That PH = -Log[H+]. *J. Chem. Educ.* **2006**, *83* (5), 752–757. https://doi.org/10.1021/ed083p752.
(42) Pines, E. *UV-Visible Spectra and Photoacidity of Phenols, Naphthols and Pyrenols*.
(43) Agmon, N. Elementary Steps in Excited-State Proton Transfer. *J. Phys. Chem. A* **2005**, *109* (1), 13–35. https://doi.org/10.1021/jp047465m.
(44) Solntsev, K. M.; Huppert, D.; Agmon, N. Photochemistry of "Super"-Photoacids. Solvent Effects. *J. Phys. Chem. A* **1999**, *103* (35), 6984–6997. https://doi.org/10.1021/jp9902295.
(45) Pines, D.; Ditkovich, J.; Mukra, T.; Miller, Y.; Kiefer, P. M.; Daschakraborty, S.; Hynes, J. T.; Pines, E. How Acidic Is Carbonic Acid? *J. Phys. Chem. B* **2016**, *120* (9), 2440–2451. https://doi.org/10.1021/acs.jpcb.5b12428.
(46) Gajst, O.; Pinto Da Silva, L.; Esteves Da Silva, J. C. G.; Huppert, D. Enhanced Excited-State Proton Transfer via a Mixed Water-Methanol Molecular Bridge of 1-Naphthol-5-

Sulfonate in Methanol-Water Mixtures. *J. Phys. Chem. A* **2018**, *122* (20), 4704–4716. https://doi.org/10.1021/acs.jpca.8b00957.
(47) Nightingale, E. R. Phenomenological Theory of Ion Solvation. Effective Radii of Hydrated Ions. *J. Phys. Chem.* **1959**, *63* (9), 1381–1387. https://doi.org/10.1021/j150579a011.